Optics Letters

Analyzing radial and azimuthal Brownian motion in Laguerre–Gaussian optical traps

Saifollah Rasouli,[1,2,*] Mohsen Samadzadeh,[1] Faegheh Hajizadeh,[1] and Sergey A. Ponomarenko[3,4]

[1]Department of Physics, Institute for Advanced Studies in Basic Sciences (IASBS), 444 Prof. Yousef Sobouti Blvd., Zanjan 45137-66731, Iran
[2]Optics Research Center, Institute for Advanced Studies in Basic Sciences (IASBS), Zanjan 45137-66731, Iran
[3]Department of Physics and Atmospheric Science, Dalhousie University, Halifax, Nova Scotia B3H 4R2, Canada
[4]Department of Electrical and Computer Engineering, Dalhousie University, Halifax, Nova Scotia B3J 2X4, Canada
*rasouli@iasbs.ac.ir

Received 5 September 2025; revised 29 October 2025; accepted 1 November 2025; posted 3 November 2025; published 12 November 2025

Optical trapping, orchestrated by intensity-gradient forces and radiation pressure, is a powerful technique in physics and nanotechnology that enables precise control and manipulation of microscopic and nanoscale particles with widespread applications in biotechnology, nanoscience, and fundamental physics research. The annular intensity profile and helical phase structure of Laguerre–Gaussian (LG) beams furnish unparalleled conditions for optical trapping, particularly, in the context of studying rotational motion of particles known as tweezing. Here, we study tweezing of dielectric particles trapped with higher-order LG beams under the strong focusing condition and in the presence of spherical aberrations. We quantify the transverse trap stiffness with the aid of two complementary approaches—Boltzmann statistics and the equipartition theorem—through a comprehensive analysis of the times series of the radial and angular position of a particle. In contrast to the quadrant photodiode (QPD) method, which is faster but has a limited field of view and requires careful calibration, our wide-field imaging-based approach provides direct distance calibration and allows accurate stiffness measurements even when the trapped particle experiences a significant slowdown or the light field distribution lacks perfect axial symmetry. The method offers several attractive advantages: (i) it enables reliable characterization of stiffness anisotropy for LG traps with topological charges up to $\ell = 7$; (ii) it remains robust in the presence of aberrations that distort the axial symmetry of the beam; and (iii) it provides insight into both radial stability and angular-velocity variations. The proposed approach can enhance the accuracy of optical trapping measurements, improve the design of high-order LG optical traps, and deepen our understanding of particle behavior in complex optical potential landscapes.

https://doi.org/10.1364/OL.577588

Optical trapping has become an essential technique for non-invasive manipulation and mechanical characterization of micro- and nano-scale particles. Among its key performance metrics, trap stiffness plays a central role in quantifying optical forces, particularly in applications across biophysics and materials science [1,2]. The optical trapping technique, which is underpinned by the intensity gradient force and radiation pressure, enables precise control over the motion and positioning of microscopic particles, making it widely applicable in biotechnology, nanoscience, and fundamental physics research.

Recent developments in structured light, especially Laguerre–Gaussian (LG) beams that carry orbital angular momentum (OAM), have opened new avenues for particle manipulation through tailored phase and intensity distributions [3–7]. The annular intensity profile and helical phase structure of LG beams create unique optical potential landscapes, enabling stable three-dimensional trapping but also imparting rotational motion to trapped particles. While conventional Gaussian beams are still commonly used for polystyrene particle trapping [8,9], the topological charges (TCs) embedded in LG beams significantly modify both transverse and axial stiffness characteristics [10].

Despite increasing interest in OAM-based trapping, the influence of higher-order TCs (e.g., $\ell = 7$) on trap stiffness and particle dynamics remains poorly understood. Previous studies on lower-order modes ($\ell = 1$–3) have shown asymmetries in stiffness and rotational motion [3,11], but systematic evaluation of stiffness behavior and stability at higher ℓ values are still lacking. In this work, we address this gap through a combined theoretical and experimental approach. We evaluate the optical trap stiffness using two complementary techniques: Boltzmann statistics and the equipartition theorem, based on precise measurements of particle fluctuations. We analyze the trapped particle motion by tracking both its radial and angular positions over time, as well as determining the radial position distribution and angular velocity. In particular, we use the statistical properties of radial fluctuations as a sensitive indicator of trap stability.

The present study relies on the established theoretical framework for calculating the stiffness of the trap for confined particles in a fluid, where light refraction occurs within the particles and spherical aberration is present [12,13]. It should be noted that in several recent publications, the stiffness of the trap was determined solely from fluctuations in the position of a particle relative to the center of the beam when trapped by a Gaussian beam. In this work, we notice a similarity between these center-

position fluctuations in Gaussian beam traps and the fluctuations of the particle position relative to its mean radial location in our LG beam experiments. This analogy allows us to adopt the same formulation for stiffness determination. A theoretical treatment specifically tailored to the present LG-beam case remains an open problem.

In our experiments, the required LG beams were generated by diffracting a Gaussian beam from homemade purely amplitude fork-shaped gratings printed on transparent plastic sheets. Experimental results reveal that, for beams with a TC greater than 3 and under strong focusing conditions (Olympus objective lens, UPlan, 100×, NA=1.3, Oil immersion), the angular velocity of trapped particles within the beam's intensity ring varies nonlinearly with azimuthal position. This angular-velocity nonuniformity is likely a consequence of spherical aberration, which has been predicted theoretically in previous works [4]. Such a phenomenon may arise from significant modifications of the optical field within the intensity ring at the focus of a high-NA lens, together with a nonlinear distribution of diffractive forces [4].

In the approach presented here, transverse trap stiffness is determined by analyzing radial position fluctuations of the trapped particle, unlike the conventional quadrant photodiode (QPD) method, which measures the position and fluctuations of the particle by detecting the intensity of scattered light across its four quadrants, but is limited by the angular collection range of the scattered light [14,15]. Our method enables accurate determination of the stiffness anisotropy of high-topological-charge LG optical traps in the focal plane, as well as their anisotropy. For instance, when the spherical aberration of a high-NA focused LG beam exceeds a certain threshold, the aberration becomes large enough to distort the beam's ring intensity distribution, breaking its circular symmetry. As a result, a particle trapped in one region of this asymmetric intensity ring may almost come to rest, with a substantial portion of its scattered light failing to reach the QPD. In contrast, our imaging-based method for measuring the radial position of the particle maintains high accuracy even when the particle exhibits a significant slowdown in the high-intensity/low-phase-gradient regions of the beam ring. It is worth noting that in [16], an imaging method was used for tailoring bistability in optical tweezers using vortex beams and spherical aberration. In that work, the trap stiffness was still estimated from the power spectral density of the x coordinate of the microsphere position.

In this study, we introduce a novel approach for quantifying the trapping strength of LG beams through a comprehensive analysis of the radial and angular fluctuations of the particle position, combined with variations in its angular velocity. As shown in Fig. 1(a), a 1064 nm laser beam is expanded and directed onto a fork grating with TCs $\ell = 4 - 7$. A 4f system, using a 40 cm focal length lens and a circular aperture at its Fourier plane, isolates the +1 order, forming an LG beam sized to fit the objective's entrance pupil. The selected order is reflected by a dichroic mirror (DM) and focused by an objective lens (Obj), forming an optical trap at the focal plane within the sample. Simultaneously, the sample is uniformly illuminated with white light from a lamp via a condenser lens (Cond.). The transmitted light passes through the DM, is reflected by mirror M2, and the image of the trapped particle is projected by imaging lens (IL) onto a camera placed at the focal plane of IL. Figures 1(b)–1(d) show the transmittance of an amplitude fork grating, along with

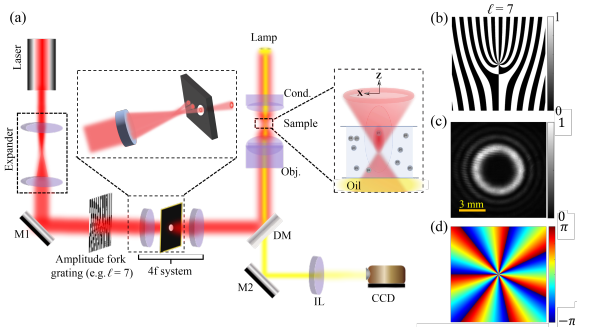

Fig. 1. (a) Schematic of the optical trapping setup. Central inset shows diffraction-order filtering at the Fourier plane of the first lens, transmitting only the +1 diffraction order. (b) Transmittance profile of an amplitude fork grating with $\ell = 7$. (c) Experimental intensity distribution, recorded before the objective, and (d) the corresponding ideal phase distribution for the +1 order LG beam.

the intensity and phase profiles of the resulting LG beam in the +1 diffraction order. All fork gratings used in this work feature a period of 2.5 lines/mm and were fabricated on a fully transparent plastic substrate with a thickness of 0.2 mm. While the TC is an intrinsic property of the fork dislocations and not the grating period, a larger period degrades beam quality.

In optical trapping, the motion of the particles is governed by the intensity gradient and radiation pressure of the laser beam. In this study, the trajectory of a single polystyrene particle (diameter 1.18 μm, in water medium) within the trap follows an approximately circular path of radius r_c. The coordinates (x_i, y_i) of the particle position were extracted as the center of mass in each frame using a high-resolution camera with a spatial precision of 59 nm/pixel at 30 fps, enabling accurate spatio-temporal tracking. (x_i, y_i) are given relative to the coordinate system whose origin is located at the corner of the laboratory camera.

The trapped particle circulates due to the OAM of the optical field. As shown in Fig. 2(a), the center of the circular trajectory (C_x, C_y) is taken as the global center of mass. We display the detected positions of the trapped particle over a 50 s interval under LG beam illumination with $\ell = 7$ in Fig. 2(b). The red line traces the overall circular trajectory of the particle, while the solid blue dots indicate its positions in individual frames. Figure 2(c) presents the corresponding radial position fluctuations over time for $\ell = 7$, revealing the stability of the circular motion. For comparison, Fig. 2(d) exhibits the positions of the detected particles over the same time period when illuminated with LG beams of $\ell = 4$, 5, and 6, demonstrating the effect of TC on the trajectory of the particle. We can infer from the figure that larger ℓ values yield larger rotation path radii, while stability decreases as a result of weaker gradient confinement. The observed path asymmetries and localized particle slowdowns likely stem from aberrations introduced by the tightly focusing objective lens, though contributions from other factors like fabrication imperfections in the fork gratings cannot be ruled out. These effects lead to asymmetries in the spatial distribution and deviations from quadratic behavior in resulting potential energy profiles, as detailed below. See also Visualization 1, Visualization 2, Visualization 3 and Visualization 4 for details.

We determine the radial and azimuthal coordinates of the particle relative to the center of its circular trajectory, corresponding

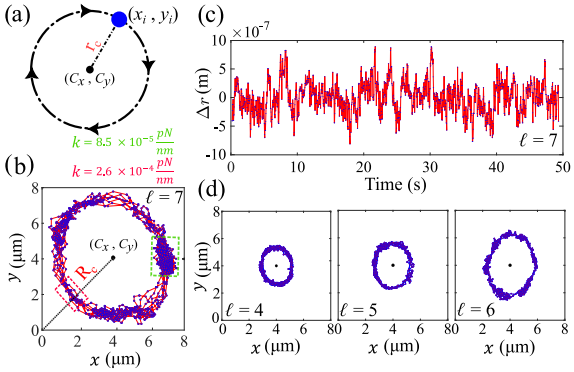

Fig. 2. (a) Schematic of the mean particle position in recorded trajectory (black dot) and its positions in individual frames (blue dots), where r_c denotes the mean trajectory radius. (b) Detected positions of the trapped particle over 50 s under LG beam illumination with $\ell = 7$; the red line traces the particle's rotation path. (c) Radial position fluctuations over time for $\ell = 7$. (d) Particle positions over 50 s under illumination with LG beams of $\ell = 4 - 6$ (See Visualization 1, Visualization 2, Visualization 3 and Visualization 4).

to its radial and angular positions in the optical trap as follows:

$$r_i = \sqrt{(x_i - C_x)^2 + (y_i - C_y)^2}, \tag{1}$$

$$\theta_i = \tan^{-1}\left(\frac{y_i - C_y}{x_i - C_x}\right), \tag{2}$$

where (C_x, C_y) is the trap center obtained from the mean particle position over the recorded trajectory, evaluated as:

$$(C_x, C_y) = \left(\frac{1}{N}\sum_{i=1}^{N} x_i,\ \frac{1}{N}\sum_{i=1}^{N} y_i\right). \tag{3}$$

The coordinates (x_i, y_i) are determined with a precision corresponding to the pixel size in each frame, followed by the analysis of the temporal evolution of (r_i, θ_i). In the measurements presented here, the particle completes approximately seven full revolutions around the circle within 50 s of observation.

The radial coordinate variation per frame, Δr_i, is:

$$\Delta r_i = r_i - r_c, \ \text{where}\ r_c = \frac{1}{N}\sum_{i=1}^{N} r_i. \tag{4}$$

r_c is the mean radius of the particle trajectory. The time series of radial variations contains information about the stability of particle motion and its deviation from the center of the ring-shaped optical trap. As shown in Fig. 2(c), these variations reveal small fluctuations caused by the interaction with a fluid that temporarily displace the particle from its ideal circular trajectory. The laser power within the sample was maintained at 11 mW.

Figures 3(a) and 3(b) show the measured angular coordinate θ_i, and its variation due to rotation with the mean angular velocity for $\ell = 7$. From a linear fit to these data, we estimate the mean angular velocity of the particle to be $\bar{\omega} = 0.90$ rad/s. Figure 3(c) shows the angular velocity as a function of azimuthal position. The data bar for each segment represents the mean angular velocity, averaged over all recorded rotations. Due to a relatively low laser power and significant focusing aberrations—primarily spherical aberration—the particle occasionally fails to maintain forward motion, causing deviations in its angular position from a perfectly uniform pattern. These aberrations distort the

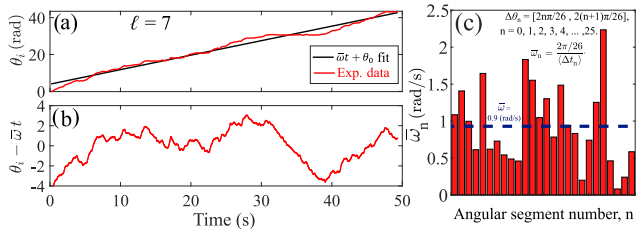

Fig. 3. (a) Angular coordinate of the particle over time. (b) Temporal variations of the angular position relative to its expected value for constant rotation. (c) Angular velocity versus azimuthal position (see Visualization 1, Visualization 2, Visualization 3 and Visualization 4).

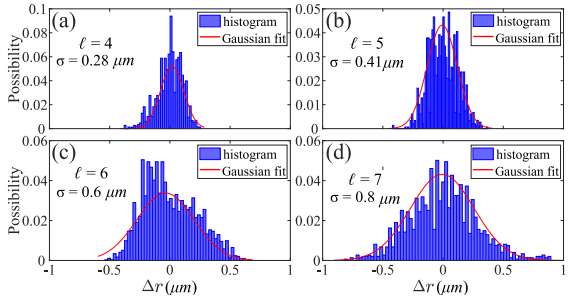

Fig. 4. Radial position distribution of the particle in the ring-shaped optical trap for TCs $\ell = 4, 5, 6, 7$.

intensity and phase gradient in the ring-shaped profile of the vortex beam. Other potential factors—including fabrication imperfections specific to each fork grating, particle and medium properties, and laser power—were considered constant to isolate the effects of TC and aberration. Visualization 1, Visualization 2, Visualization 3 and Visualization 4 show the measured $\bar{\omega}$ values for $\ell = 4 - 6$, demonstrating the non-uniform motion.

In Fig. 4, we present the radial position distribution of the particle in the ring-shaped optical trap for TCs $\ell = 4 - 7$. For each case, we fitted the histogram of radial positions with a Gaussian function to quantify the confinement of the particle in the radial direction. For $\ell = 7$, the fit yields a full width at half maximum (FWHM) of 0.62 μm, which characterizes the spatial extent of particle motion along the radial direction within the optical trap. We computed the distribution width using a kernel density estimation with Silverman's rule [17], which provides an accurate estimate of the probability density function. A comparison across different TCs shows that the radial confinement is slightly dependent on ℓ, with higher-order beams generally producing marginally broader distributions due to their larger ring radii.

We quantified the radial (transverse) stiffness of the optical trap through statistical analysis of the Brownian motion of the particle in the radial direction. The equipartition theorem offers a direct means to determine the stiffness of the trap without requiring prior knowledge of the medium viscosity or the geometry of the particle, relying solely on accurate position calibration of the detection system. For a particle in thermal equilibrium with its surroundings, the theorem states that:

$$\frac{1}{2}k\langle \Delta r^2 \rangle = \frac{1}{2}k_B T, \tag{5}$$

where k is the trap stiffness (pN/nm), $\langle \Delta r^2 \rangle$ is the variance of radial displacement, k_B is the Boltzmann constant

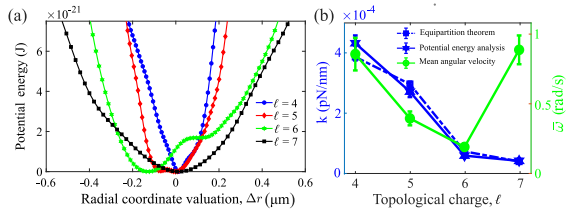

Fig. 5. (a) Measured potential energy profiles. Stiffness values were obtained from parabolic fits. (b) Trap stiffness calculated from the harmonic potential fit and Boltzmann statistics, and measured mean angular velocity for TCs $\ell = 4 - 7$.

(1.38×10^{-23} J/K), and T is the absolute temperature (298 K in our experiment). The radial displacement variance was calculated from 1,500 position measurements (30 fps over 50 s) as:

$$\langle \Delta r^2 \rangle = \frac{1}{N} \sum_{i=1}^{N} (r_i - r_c)^2 , \tag{6}$$

where r_i and r_c are given by Eqs. (1) and (4), respectively. For $\ell = 7$, from the measured displacement variance, we obtain:

$$k = \frac{k_B T}{\langle \Delta r^2 \rangle} = (5.3 \pm 0.2) \times 10^{-5} \text{ pN/nm}. \tag{7}$$

To validate this result, we alternatively extracted the trap stiffness from the optical potential energy profile using Boltzmann statistics:

$$U(\Delta r) = -k_B T \ln [P(\Delta r)] + \text{const}, \tag{8}$$

where $P(\Delta r)$ is the probability density of finding with radial displacement Δr from the trap center. We obtained the probability distribution from particle tracking data, converted to potential energy via Eq. (7), and fitted with a harmonic form as:

$$U(\Delta r) = \frac{1}{2} k \Delta r^2 . \tag{9}$$

Using the position distributions presented in Fig. 4, we show the corresponding potential energy plots in Fig. 5(a). For $\ell = 7$, fitting the parabolic potential well yielding:

$$k = (5.8 \pm 0.4) \times 10^{-5} \text{ pN/nm}, \tag{10}$$

which is in excellent agreement with the value from the equipartition theorem. Errors are evaluated based on uncertainties in time, position, temperature, and fitting statistics. From the radial position distributions in the high- (red dashed) and low-angular-velocity (green dashed) regions of Fig. 2(b), we obtained $k = 2.6 \times 10^{-4}$ and 8.5×10^{-5} pN/nm, respectively, revealing stiffness asymmetry. Figure 5(b) presents the trap stiffness, obtained from both the equipartition method and Boltzmann statistics method, as well as the angular velocity for $\ell = 4 - 7$. The trap stiffness decreases monotonically with increasing TC, as the expanding intensity ring weakens the radial optical confinement, an effect that may be further enhanced by spherical aberrations. In contrast, the angular velocity follows a non-monotonic trend: while a higher TC enhances the phase gradient, nonlinear drag due to optical potential imperfections (see $\ell = 5$ and $\ell = 6$ in Fig. 5(a)) counteracts this effect, reaching its maximum at $\ell = 6$.

In conclusion, we have experimentally investigated the trapping stiffness and tweezing dynamics of dielectric particles in LG traps with higher-order TCs under strong focusing and in the presence of spherical aberrations. By drawing on an analogy with trapping with Gaussian beams, we applied established stiffness formulations and quantified stiffness anisotropy using Boltzmann statistics and the equipartition theorem. Our imaging-based method enables accurate measurements up to $\ell = 7$ even in the presence of beam asymmetries or particle slowdown, overcoming limitations of the conventional QPD approach. Our findings offer valuable insight into the behavior of trapped particles in complex optical potentials and serve as a practical guide to help optimize higher-order LG optical traps.

Funding. Institute for Advanced Studies in Basic Sciences (G2025IASBS12632); Center for International Scientific Studies and Collaboration (CISSC) (4020667); Iran National Science Foundation (4037534).

Acknowledgment. SR conceptualized, designed, and supervised the research; established the methodology; validated the results; secured funding; and managed the project. MS, under the continuous guidance of SR and FH, performed the experiments. SR and MS analyzed the data, performed investigations, and prepared the figures and visualizations. SR wrote the manuscript. FH and SAP reviewed the manuscript and validated the results.

Disclosures. The authors declare no conflicts of interest.

Data availability. No data were generated or analyzed in the presented research.

REFERENCES

1. S. E. S. Spesyvtseva and K. Dholakia, ACS Photonics **3**, 719 (2016).
2. P. Zijlstra and M. Orrit, Rep. Prog. Phys. **74**, 106401 (2011).
3. I. Gómez-Viloria, A. Nodar, M. Molezuelas-Ferreras, *et al.*, ACS Photonics **11**, 626 (2024).
4. Y. Li, L.-M. Zhou, and N. Zhao, Opt. Lett. **46**, 106 (2021).
5. A. A. Kovalev, V. V. Kotlyar, and A. P. Porfirev, Opt. Lett. **41**, 2426 (2016).
6. J. Bayat, F. Hajizadeh, A. M. Khazaei, *et al.*, Sci. Rep. **10**, 11721 (2020).
7. P. Y. Moghadam, S. Rasouli, F. Hajizadeh, *et al.*, Opt. Express **31**, 43490 (2023).
8. M. Shiddiq, Z. Nasir, and D. Yogasari, in *AIP Conference Proceedings* (American Institute of Physics, 2013), Vol. **1555**, p. 24.
9. M. Sarshar, W. T. Wong, and B. Anvari, J. Biomed. Opt. **19**, 115001 (2014).
10. M. A. Shukri and F. M. Thabit, Phys. Scripta **99**, 065504 (2024).
11. J. So and J.-M. Choi, J. Korean Phys. Soc. **68**, 762 (2016).
12. R. R. Dorizzi and Z. Ulanowski, J. Quant. Spectrosc. Radiat. Transf. **110**, 1483 (2009).
13. K. C. Vermeulen, G. J. L. Wuite, G. J. M. Stienen, *et al.*, Appl. Opt. **45**, 1812 (2006).
14. M. Dienerowitz, G. Gibson, R. Bowman, *et al.*, Opt. Express **19**, 24589 (2011).
15. Y. Liang, Y. Cai, Z. Wang, *et al.*, Appl. Opt. **57**, 3618 (2018).
16. A. L. da Fonseca, K. Diniz, P. B. Monteiro, *et al.*, Phys. Rev. Res. **6**, 023226 (2024).
17. B. W. Silverman, *Density Estimation for Statistics and Data Analysis* (Routledge, 2018).